

DomainForensics: Exposing Face Forgery across Domains via Bi-directional Adaptation

Qingxuan Lv, Yuezun Li, Junyu Dong, Sheng Chen, *Life Fellow, IEEE*, Hui Yu, Huiyu Zhou, Shu Zhang

Abstract—Recent DeepFake detection methods have shown excellent performance on public datasets but are significantly degraded on new forgeries. Solving this problem is important, as new forgeries emerge daily with the continuously evolving generative techniques. Many efforts have been made for this issue by seeking the commonly existing traces empirically on data level. In this paper, we rethink this problem and propose a new solution from the unsupervised domain adaptation perspective. Our solution, called *DomainForensics*, aims to transfer the forgery knowledge from known forgeries (fully labeled source domain) to new forgeries (label-free target domain). Unlike recent efforts, our solution does not focus on data view but on learning strategies of DeepFake detectors to capture the knowledge of new forgeries through the alignment of domain discrepancies. In particular, unlike the general domain adaptation methods which consider the knowledge transfer in the semantic class category, thus having limited application, our approach captures the subtle forgery traces. We describe a new bi-directional adaptation strategy dedicated to capturing the forgery knowledge across domains. Specifically, our strategy considers both forward and backward adaptation, to transfer the forgery knowledge from the source domain to the target domain in forward adaptation and then reverse the adaptation from the target domain to the source domain in backward adaptation. In forward adaptation, we perform supervised training for the DeepFake detector in the source domain and jointly employ adversarial feature adaptation to transfer the ability to detect manipulated faces from known forgeries to new forgeries. In backward adaptation, we further improve the knowledge transfer by coupling adversarial adaptation with self-distillation on new forgeries. This enables the detector to expose new forgery features from unlabeled data and avoid forgetting the known knowledge of known forgery. Extensive experiments demonstrate that our method is surprisingly effective in exposing new forgeries, and can be plug-and-play on other DeepFake detection architectures.

Index Terms—Digital Forensics, DeepFake Detection, Domain-Forensics.

I. INTRODUCTION

The ever-growing convolutional neural network (CNN) based generative models [1]–[6] have made face forgery much easier than ever before, allowing people to manipulate the face’s identity, appearance and attributes in high realism with

Corresponding authors: Yuezun Li and Junyu Dong

Q. Lv, Y. Li, J. Dong and S. Zhang are with the College of Computer Science and Technology, Ocean University of China, Qingdao 266100, China (E-mails: lvqingxuan@stu.ouc.edu.cn, liyuezun@ouc.edu.cn, dongjunyu@ouc.edu.cn, zhangshu@ouc.edu.cn).

S. Chen is with School of Electronics and Computer Science, University of Southampton, Southampton SO17 1BJ, U.K., and also with the College of Computer Science and Technology, Ocean University of China, Qingdao 266100, China (E-mail: sqc@ecs.soton.ac.uk).

H. Yu is with School of Creative Technologies, Faculty of Creative and Cultural Industries, University of Portsmouth, Portsmouth PO1 2DJ, U.K. (E-mail: hui.yu@port.ac.uk).

H. Zhou is with School of Computing and Mathematic Sciences, University of Leicester, Leicester LE1 7RH, U.K. (E-mail: hz143@leicester.ac.uk).

little effort. These CNN-based face forgery techniques, known as *DeepFake*, have drawn much attention, as their abuse using can lead to impersonation videos, economic fraud, biometric attacks, and even national security problems [7]. Thus, it is urgent and important to counteract the misuse of DeepFakes.

During the past few years, large number of DeepFake detection methods [8]–[12] have emerged. Trained on the recently proposed large DeepFake datasets, such as FaceForensics++ (FF++) [13] and Celeb-DF [14], these detection methods have shown promising performance. However, these methods fall into the category that the training and testing sets are from the same distribution, e.g., the same type of forgery or the same dataset, which unfortunately limits their practical applications, as there are always new types of forgeries emerging continuously and widespreading to everywhere on various social platforms. These new types of forgeries are very unlikely to have been included in the existing datasets, and thus they are unseen to these detectors, causing significant performance degradation (see Fig. 1 top part). This circumstance gives rise to a big challenge to DeepFake detectors, that is, how to detect constantly emerging new forgeries.

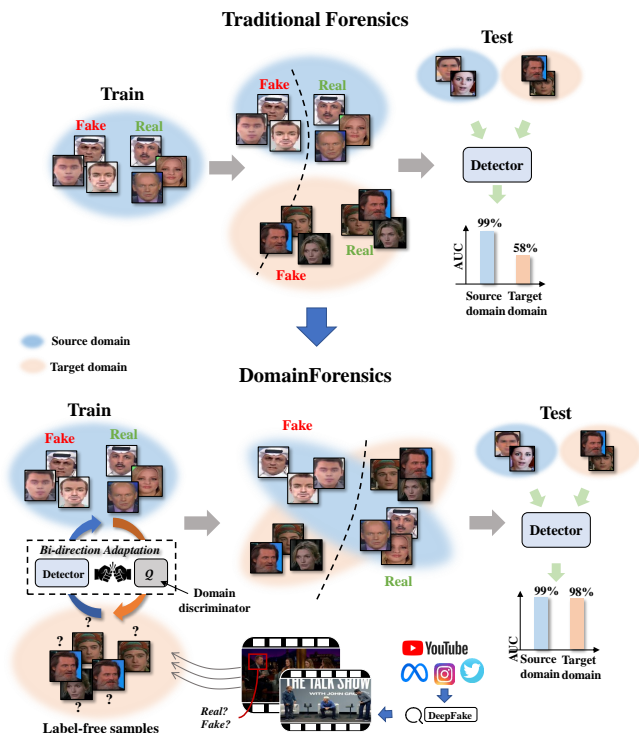


Fig. 1. Overview of traditional forensics (top) and *DomainForensics* (bottom). Traditional forensics achieves excellent performance on known forgeries but performs poorly on new forgeries. In contrast, *DomainForensics* can effectively expose new forgeries by performing the proposed bi-directional adaptation, which can learn the common forgery features across domains using adversarial training.

Recently, attempts have been made in the literature to solve this issue. One typical line of research is to use a variety of data augmentation to increase the generalization ability [15]–[18]. These methods usually create forged faces by augmenting the pristine videos to cover the known types of forgeries as much as possible. Despite of the promisingly improved generalization, the types of augmentation are limited to known forgeries, thus hindering the performance when confronting unseen forgeries. Frequency clue is also used to improve generalization ability [19]–[22]. However, this clue is easily affected by data processing and highly correlated with video quality, which cannot perform consistently across different datasets. A different direction of research is to apply transfer learning, such as zero- and few-shot learning [23]–[25], to improving generalization on new forgeries. Since zero-shot learning cannot access the samples of new forgeries in training, its performance is highly suppressed. In contrast, few-shot learning methods relax the restrictions in that they can access a few samples of new forgeries in training. However, this requires the annotation of these samples, which may not be easily obtained in practice, as we may not know whether a face is forged or not, e.g., multiple faces are in view but only video-level labels are provided. Thus, a fundamental question is: *can we detect new forgeries by only accessing target samples without any labels, while achieving competitive performance?*

In this paper, we cast DeepFake detection into a new formulation as an *unsupervised domain adaptation* problem, by transferring the knowledge from the source domain to the target domain, without using any annotations of target samples in training. This is very different from the existing strategies and it offers significant advantages over them. Specifically, for DeepFake detection, we can treat the known forgeries as the source domain and new forgeries as the target domain, see Fig. 1 bottom part. Our goal is to push the DeepFake detector to learn the common forgery features across different domains by only using label-free interested video collections. It is worth noting that this DeepFake detection problem has a significant discrepancy with the general unsupervised domain adaptation problem, as we aim to learn the common forgery feature from the same category of faces (real or fake), which is more subtle than the semantic features of different categories in the general unsupervised domain adaptation problem (e.g., cat, dog, etc.). To this end, we propose a new unsupervised domain adaptation framework, called *DomainForensics*, for DeepFake detection. The key to our *DomainForensics* is a novel *bi-directional adaptation* strategy. This is very different from the existing DeepFake detection framework which only considers one direction to learn the knowledge supervised by the source domain and transfer it to the target domain. However, since the forgery features are subtle, the one-directional adaptation will inevitably lose a certain amount of knowledge [26]–[28], thus limiting the achievable performance on the target domain. To overcome this problem, we design bi-directional adaptation, which first transfers the knowledge from the source domain to the target domain, referred to as forward adaptation, and then reverses the adaptation from the target domain to the source domain, called backward adaptation. The backward adaptation stage utilizes the results of the forward adaptation

stage, further explores the knowledge from the target domain, and transfers it back to the source domain. With the mutual adaptation, DeepFake detector can fully grab the common forgery features across domains.

To verify our idea, we adopt Vision Transformer (ViT) [29] as our DeepFake detector in the experiment, due to its successful application on vision tasks. Other architectures, such as ResNet [30], Xception [31] and EfficientNet [32], can also be used in our framework, and this will also be demonstrated. Since the frequency space can reveal the forgery traces [19], [20], we use color images and corresponding frequency-transformed maps as the input. In the forward adaptation stage, we develop a discriminator that is trained together with the DeepFake detector in an adversarial manner, where the discriminator aims to tell which domain the learned feature is from, and the DeepFake detector aims to extract features that confuse the discriminator. By doing so, the distribution of the target domain is pulled close to the source domain. In the backward adaptation stage, the adaptation is reverted. Since no labels are provided, we employ self-distillation [27] to further excavate the knowledge of the target domain, and then apply the adversarial training to the distilled model, in order to transfer the knowledge back to the source domain. Extensive experiments are conducted on FF++ and Celeb-DF datasets in several cross-domain scenarios, including different manipulation methods, datasets and types, to demonstrate the effectiveness of our method.

The contribution of this work is summarized as follows.

- 1) We propose a new DeepFake detection solution called *DomainForensics* to handle continuously emerged new forgeries. Different from recent efforts, our method focuses on pushing the detectors to learn the common forgery features across domains, that is, to transfer the forgery knowledge from known forgeries to unseen forgeries, instead of seeking the empirical-common traces on the data level.
- 2) We propose a new bi-directional adaptation strategy, which first transfers the forgery knowledge from the source domain to the target domain in forward adaptation, and then reverses the adaptation from the target domain to the source domain in backward adaptation. Since the forgery traces are very subtle, we design the backward adaptation stage to further refine the results obtained from the forward adaptation stage with a self-distillation scheme.
- 3) Extensive experiments are conducted on FF++ and Celeb-DF datasets with several cross-domain scenarios, including crossing manipulation methods, crossing datasets, and crossing generative types, to demonstrate the effectiveness of our method. We also study the effects of various adaptation settings, various amounts of training samples and different components, to provide thoughtful insights for the following research.

The remainder of this paper is organized as follows. Section II reviews the recent works on DeepFake detection and unsupervised domain adaptation. Section III details our proposed *DomainForensics*, including the problem formulation, network

framework and bi-directional adaptation. Section IV offers extensive experiments and elaborates on the experimental results. The paper concludes in Section V.

II. RELATED WORK

In this section, we first present an overview of the existing deepfake detection approaches. We then provide a brief review of unsupervised domain adaptation and discuss the differences between the previous works and our approach.

A. Deepfake Detection

With the advent of large-scale DeepFake datasets, e.g., [13], [14], DeepFake detection has made significant progress in recent years, e.g., [8]–[12], [16], [18], [33]–[37]. One challenging problem in this task is how to detect constantly emerging new forgeries. The methods [15]–[18], [35], [38] enhance generalization ability by exploring elaborate augmentations on pristine videos, with the aim of covering most of the known forgery types. The limitation of these methods is that the augmentation diversity is restricted to known forgeries. Hence, these methods can hardly handle unknown forgeries. Another vein of methods [10], [19]–[22], [39], [40] utilize frequency features to improve generalization ability. However, frequency features can easily be disrupted by post-processing such as compression [41]. Inspired by transfer learning, the methods [23]–[25], [37] employ zero-shot and few-shot learning to detect new forgeries. Since zero-shot learning cannot access the samples of new forgeries, its performance gain is severely limited. The few-shot learning needs a small portion of samples and corresponding labels of new forgeries. However, although the video-level label is easily obtained, the face-level label is extremely difficult to obtain in practice.

B. Unsupervised Domain Adaptation

Unsupervised domain adaptation (UDA) aims to address the challenge of transferring knowledge from a source domain to a target domain when labeled data is scarce or completely absent in the target domain. Ben-David *et al.* [42] theoretically revealed that the cross-domain common features serve as latent representations that encapsulate shared and domain-common features across diverse domains. The primary objective is to diminish or eliminate domain-specific variations while retaining domain-agnostic information. The acquisition of cross-domain common representation enhances the model’s reliability to domain shifts by prioritizing task-relevant information that transcends domain-specific discrepancies. Consequently, the model achieves improved generalization to unlabeled target domains, even in the scenarios with limited available data.

The existing works for addressing UDA can be classified to two main forms, namely, the discrepancy-based approach and the adversarial approach. Concretely, discrepancy-based methods encourage the model to align the domain discrepancy by minimizing the metrics that can measure the distribution discrepancy between the source and target domains [43]–[46]. Inspired by the success of generative adversarial network (GAN) [47], recently developed works employed extra

adversarial discriminator to align the domain discrepancy, as the feature distributions of source and target domains can be matched by means of confusing the discriminator [48]–[50]. In addition, some state-of-the-art methods build up the feature extractor based on modern transformer structure [51]–[53], which demonstrates that UDA not only helps traditional CNNs to improve the generalization but also is profitable for transformer-based networks. This motivates us to treat the transformer networks as the cornerstone structure and further explore effective UDA methods for face forgery detection.

Note that the general UDA task targets transferring the knowledge of the semantic class category. By contrast, our approach differs from the aforementioned UDA methods in that we aim to explore the subtle forgery features in the face category only. We also find that the existing adaptation schemes, which only consider the adaptation from the source domain to the target domain, is unlikely to perform well on our task. In contrast, our proposed bi-directional adaptation strategy can further explore the knowledge from the unlabeled data in the target domain, as such mutual adaptation coupled with knowledge transfer with self-distillation enables the model to learn common forgery features across known and new forgeries. To the best of our knowledge, Chen and Tan [54] is the first work that attempted to solve Deepfake detection using unsupervised domain adaptation. However, it is a trivial usage of a naive existing solution without improvement, and hence the detection performance is not satisfied. By contrast, our *DomainForensics* adopts a meticulously designed strategy, named bi-directional adaptation, which can fully learn the common forgery features across domains and it is validated under several practical cross-domain scenarios.

III. DOMAINFORENSICS

To achieve continuously exposing new forgeries, we formulate DeepFake detection into an unsupervised domain adaptation problem, which transfers the forgery features from known forgeries to new forgeries, without the need of target labeling. Since the forgery features are very subtle, adapting the general UDA to our task is difficult. As such, we propose a new bi-directional adaptation strategy to fully explore the common forgery features across domains. It is worth noting that our *DomainForensics* is plug and play, i.e., it can be applied to other DeepFake detection architectures.

We start with the problem formulation in Subsection III-A, and then discuss the advantages of our *DomainForensics* over other architectures in Subsection III-B, followed by a performance comparison with existing UDA schemes in Subsection III-C. This naturally motivates us to introduce the new bi-directional adaptation strategy in Subsection III-D and our network architecture in Subsection III-E.

A. Problem Formulation

Let the sets of known forgeries and new forgeries corresponding to two different domains be denoted as the source domain \mathcal{D}_s and target domain \mathcal{D}_t , respectively. The source domain \mathcal{D}_s is fully annotated as $\mathcal{D}_s = \{(x_i^s, y_i^s)\}_{i=1}^{n_s}$, where (x_i^s, y_i^s) is the i -th pair of sample and its corresponding label

(i.e., real or not), and n_s is the number of samples. Differently, the target domain \mathcal{D}_t only contains samples without any annotations, which are given by $\mathcal{D}_t = \{x_i^t\}_{i=1}^{n_t}$, where n_t is the number of samples. Each domain can be divided into a training set and a testing set as $\{\mathcal{D}'_s, \mathcal{D}''_s\}$ and $\{\mathcal{D}'_t, \mathcal{D}''_t\}$, respectively. We employ \mathcal{D}'_s and \mathcal{D}'_t in the training phase and perform evaluation on \mathcal{D}''_s and \mathcal{D}''_t in the testing phase. Note that \mathcal{D}''_s and \mathcal{D}''_t are unseen during training.

Denote a DeepFake detector as $\mathcal{H} = \mathcal{G} \circ \mathcal{F}$, where \mathcal{G} is the classifier and \mathcal{F} is the feature extractor. Given a face image x , the output logits of DeepFake detector \mathcal{H} can be defined as $\mathcal{G}(\mathcal{F}(x; \theta_{\mathcal{F}}); \theta_{\mathcal{G}})$, where $\theta_{\mathcal{F}}$ and $\theta_{\mathcal{G}}$ are the parameters of the feature extractor and classifier, respectively. The challenge under this scenario lies in transferring the forgery knowledge learned from known forgeries \mathcal{D}_s to new forgeries \mathcal{D}_t , in terms of the underlying marginal distribution discrepancy, i.e., different manipulated approaches. Our goal is to push the feature extractor to learn the common forgery features across different domains, without the supervision of target labels, i.e., achieving favorable performance on both \mathcal{D}''_s and \mathcal{D}''_t .

B. DomainForensics versus Existing Architectures

Using data augmentation is the most typical solution to improve the generalizability of detection methods, e.g., FWA [55], Face X-ray [16], SBI [18]. These methods attempt to synthesize various pseudo-fake faces to cover known forgery as much as possible. By training on these augmented samples, the detectors can learn the common forgery features. In this scenario, the manipulation operations of new forgeries should be known as a prior, in order to synthesize the applicable pseudo-fake faces. However, the technical details of new forgeries may not be accessible in reality, limiting the application of these existing methods. In our scenario, we do not require the technical details of new forgeries. Instead, we can collect a set of videos that contains new forgery faces, and simply extract all faces in a video without knowing the label (real or fake) of faces. Using these samples, we can align the detectors to learn the transferable knowledge from the known forgery to this new forgery.

This scenario is practical and useful. For example, we can obtain video sets by searching the keywords, e.g., DeepFake, on video platforms. The obtained videos are likely a mix of real and fake faces due to the natural deviation of search engines, i.e., we cannot ensure whether a video that appeared in search results is real or fake. Even though the search results are perfectly matched, i.e., the video-level annotation is correct, the obtained faces can still be mixed, as a video usually contains multiple faces and we cannot know which face is real or fake if only video-level annotation is given. Under this practical circumstance, our method can expose new forgeries with these unlabeled samples.

C. Comparison with Existing UDA Schemes

To learn domain-common forgery features, we consider building up a solution from the perspective of UDA. With the aim of reducing the domain discrepancy, early domain adaptation methods put eyes on transferring knowledge from

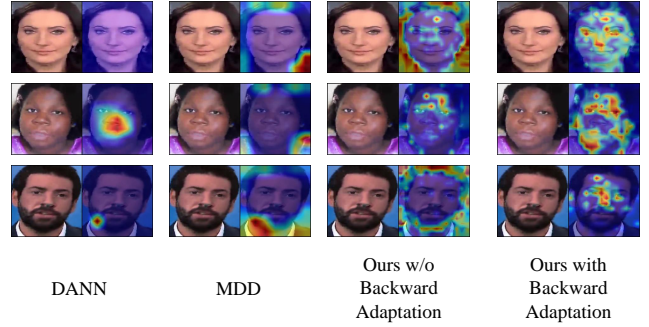


Fig. 2. Grad-CAM visualization. We train the models, including DANN [48], MDD [46] and our *DomainForensics*, and visualize the activation maps on FF++ dataset under FS→F2F scenario. These figures show that models fails to fully capture the common forgery features when only employing one-directional adaptation.

the source domain to the target domain [45], [46], [48]. However, such one-direction adaptation methods are insufficient in digging out the subtle forgery knowledge from unlabeled target data. Fig. 2 shows several examples of the feature activation maps visualized by Grad-CAM [56] using one-direction adaptation. The first two columns from left to right show the CAMs of DANN [48] and MDD [46], two typical domain adaptation methods. The last two columns are the CAMs of our approach without and with backward adaptation. It can be seen that the typical one-direction domain adaptation cannot locate the forgery features very well in these examples, either paying attention to the background area or the central local face part. In comparison, the CAMs of our method trained with backward adaptation scatter all around the whole face, activating more correct forgery features than these methods including ours without using backward adaptation. This illustration demonstrates that using existing domain adaptation methods for our task is questionable and inspires us to develop a devoted solution, which we detail in the following subsection.

D. Bi-directional Adaptation

As aforementioned, to learn domain-common forgery features, we consider building up a solution from the perspective of UDA. Existing general domain adaptation usually considers one-direction to transfer knowledge from the source domain to the target domain. However, such a one-direction adaptation is insufficient in learning transferable knowledge, as it neglects to learn from unlabeled target data, as demonstrated in the previous subsection. Thus, we propose a new bi-directional adaptation strategy, which consists of both forward adaptation and backward adaptation. The forward adaptation stage aims to transfer the knowledge from the source domain to the target domain, just as the existing solutions [45], [48], [49]. However, due to the limitation of such a one-direction adaptation, a portion of target domain knowledge is lost in the transfer, thus hindering the performance of the target domain. To eliminate or mitigate this deficiency, we develop a backward adaptation stage to fine-tune the DeepFake detector on the target domain, while retaining the learned knowledge in the forward adaptation stage. Fig. 3 illustrates the proposed bi-directional adaptation strategy.

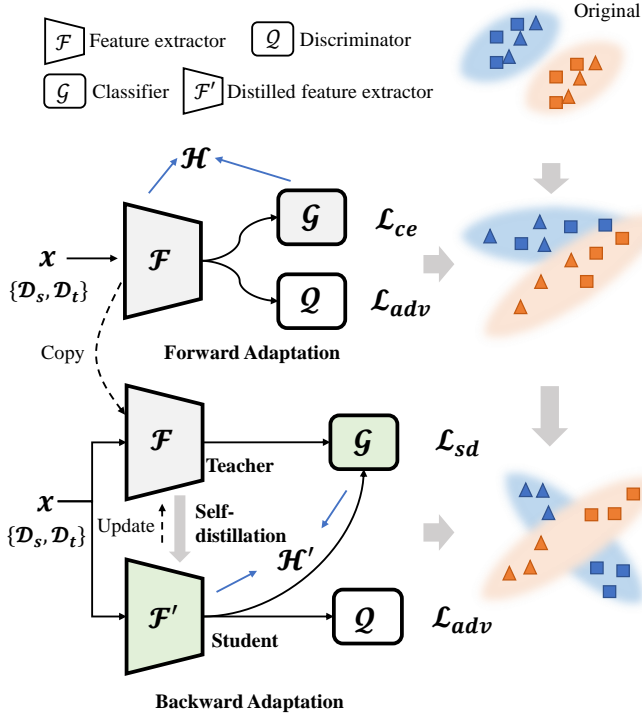


Fig. 3. Illustration of the proposed bi-directional adaptation strategy, containing forward adaptation and backward adaptation with \mathcal{H}' as the final DeepFake detector. Note that other architectures can also be used in our framework.

1) *Forward Adaptation*: In this stage, we aim to learn the common forgery features by adapting the source domain to the target domain. Concretely, we design two loss terms. The first term is a cross-entropy loss \mathcal{L}_{ce} , which trains the DeepFake detector on the fully-annotated source domain:

$$\min_{\theta_{\mathcal{F}}, \theta_{\mathcal{G}}} \mathcal{L}_{ce} = \mathbb{E}_{(x_i^s, y_i^s) \sim \mathcal{D}_s} \left[-\log \mathcal{G}(\mathcal{F}(x_i^s; \theta_{\mathcal{F}}); \theta_{\mathcal{G}})^{y_i^s} \right]. \quad (1)$$

This loss term enables the DeepFake detector to distinguish classes, i.e., telling apart real and fake faces. To transfer this knowledge from the source domain to the target domain, the essence of this stage is to push the feature extractor \mathcal{F} to generate features that cannot be identified from which domain they come. To achieve this goal, we design an adversarial loss \mathcal{L}_{adv} as the second loss term, which guides the training of feature extractor \mathcal{F} with a discriminator \mathcal{Q} in an adversarial manner. Denote $\theta_{\mathcal{Q}}$ as the parameters of discriminator \mathcal{Q} . This loss term can be defined as

$$\min_{\theta_{\mathcal{F}}} \max_{\theta_{\mathcal{Q}}} \mathcal{L}_{adv} = \mathbb{E}_{x_i^s \sim \mathcal{D}_s} \left[\log \mathcal{Q}(\mathcal{F}(x_i^s; \theta_{\mathcal{F}}); \theta_{\mathcal{Q}}) \right] + \mathbb{E}_{x_i^t \sim \mathcal{D}_t} \left[\log (1 - \mathcal{Q}(\mathcal{F}(x_i^t; \theta_{\mathcal{F}}); \theta_{\mathcal{Q}})) \right]. \quad (2)$$

The discriminator \mathcal{Q} outputs binary labels, i.e., $\mathcal{Q}(\cdot; \theta_{\mathcal{Q}}) \in \{0, 1\}$, where 0 denotes target domain and 1 denotes source domain. The overall loss of this stage is written as

$$\mathcal{L}_{fas} = \alpha_1 \cdot \mathcal{L}_{ce} + \alpha_2 \cdot \mathcal{L}_{adv}, \quad (3)$$

where α_1 and α_2 are the weight factors. The training of this stage is an adversarial min-max game between feature extractor \mathcal{F} and discriminator \mathcal{Q} . To update \mathcal{F} , we fix the parameters of \mathcal{Q} , and vice versa. Note that in the optimization of \mathcal{L}_{adv} , we do not need any class labels from both domains.

2) *Backward Adaptation*: The existing adaptation methods usually only consider the one-direction forward adaptation and their performance are limited on our task due to the loss of knowledge in transferring. The key to overcome this limitation is to mine effective forgery features more specific to the target domain. Concretely, we reverse the adaptation by training the DeepFake detector on the target domain and then transferring the knowledge from the target domain back to the source domain. The major challenge here is that no labels are provided in the target domain, and thus we cannot refine the DeepFake detector in the form of cross-entropy loss \mathcal{L}_{ce} that is used in the forward adaptation stage.

To address this difficulty, we adopt self-distillation in our framework to further explore the specific representations of the target domain. Inspired by SIMCLRv2 [27], we employ a teacher-student network model as the training structure. Specifically, during the training process, we adopt the feature extractor \mathcal{F} with the parameters $\theta_{\mathcal{F}}$ and the classifier \mathcal{G} with the parameters $\theta_{\mathcal{G}}$ used in the forward adaptation stage as the teacher model. We then create a new feature extractor \mathcal{F}' with the parameters $\theta_{\mathcal{F}'}$, which has the same model structure as \mathcal{F} and whose parameters $\theta_{\mathcal{F}'}$ are initialized with the same parameters as \mathcal{F} . \mathcal{F}' is combined with the classifier \mathcal{G} to make up the student model. It can be seen that the teacher and student models use the same model structure.

Concretely, the self-distillation loss \mathcal{L}_{sd} is defined as

$$\min_{\theta_{\mathcal{F}}, \theta_{\mathcal{F}'}, \theta_{\mathcal{G}}} \mathcal{L}_{sd} = -\sum_{x_i^t \in \mathcal{D}_t} \left(\sum_k \mathcal{P}(k|x_i^t; \tau) \log \mathcal{P}'(k|x_i^t; \tau) \right). \quad (4)$$

Here \mathcal{P} and \mathcal{P}' are the distillation probabilities of the teacher model and student model, respectively. In particular,

$$\mathcal{P}(k|x_i; \tau) = \frac{\exp(\mathcal{G}(\mathcal{F}(x_i; \theta_{\mathcal{F}}); \theta_{\mathcal{G}})^k / \tau)}{\sum_{k'} \exp(\mathcal{G}(\mathcal{F}(x_i; \theta_{\mathcal{F}}); \theta_{\mathcal{G}})^{k'} / \tau)}, \quad (5)$$

where k is the class index and τ is a scalar temperature parameter. $\mathcal{P}'(k|x_i; \tau)$ is obtained by replacing \mathcal{F} with \mathcal{F}' in (5). Minimizing this loss helps the student model to excavate more knowledge from the target domain. To achieve the knowledge transfer, we utilize the adversarial loss \mathcal{L}_{adv} as described in the forward adaptation stage on the same discriminator \mathcal{Q} and the distilled feature extractor \mathcal{F}' . The overall loss of this stage is the combination of these two loss terms as

$$\mathcal{L}_{bas} = \alpha_3 \cdot \mathcal{L}_{sd} + \alpha_4 \cdot \mathcal{L}_{adv}, \quad (6)$$

where α_3 and α_4 are weight factors. We optimize this loss adversarially as in the forward adaptation stage. At the end of each training epoch, we update the teacher model by copying the parameters of the student model to the teacher model:

$$\theta_{\mathcal{F}} = \theta_{\mathcal{F}'}. \quad (7)$$

This backward adaptation strategy provides more accurate guidance from the teacher model, thus promoting the student model to learn more knowledge. Both the self-distillation loss \mathcal{L}_{sd} and adversarial loss \mathcal{L}_{adv} do not need any class labels from both domains.

Algorithm 1 Training procedure of bi-directional adaptation

Input: Source domain \mathcal{D}'_s ; Target domain \mathcal{D}'_t ; Initial feature extractor \mathcal{F} with parameters $\theta_{\mathcal{F}}$; Initial classifier \mathcal{G} with parameters $\theta_{\mathcal{G}}$; Initial distilled feature extractor \mathcal{F}' with parameters $\theta_{\mathcal{F}'}$; Initial discriminator \mathcal{Q} with parameters $\theta_{\mathcal{Q}}$; Number of forward adaptation epochs T_1 ; Number of backward adaptation epochs T_2

// Forward adaptation stage

while $t \leq T_1$ **do** $\triangleright t = 0$

// Fix \mathcal{Q}

$\min_{\theta_{\mathcal{F}}, \theta_{\mathcal{G}}} \alpha_1 \cdot \mathcal{L}_{ce} + \alpha_1 \cdot \mathcal{L}_{adv}$

// Fix \mathcal{F}, \mathcal{G}

$\max_{\theta_{\mathcal{Q}}} \mathcal{L}_{adv}$

end while

// Backward adaptation stage

while $t \leq T_2$ **do** $\triangleright t = 0$

// Fix \mathcal{Q}

$\min_{\theta_{\mathcal{F}}, \theta_{\mathcal{F}'}, \theta_{\mathcal{G}}} \alpha_3 \cdot \mathcal{L}_{sd} + \alpha_4 \cdot \mathcal{L}_{adv}$

// Fix $\mathcal{F}, \mathcal{F}', \mathcal{G}$

$\max_{\theta_{\mathcal{Q}}} \mathcal{L}_{adv}$

// Update \mathcal{F}

$\theta_{\mathcal{F}} = \theta_{\mathcal{F}'}$

end while

Output: $\mathcal{F}', \mathcal{G}$

3) *Training and Inference:* The training procedure of our framework is summarized in Algorithm 1. In inference, we use feature extractor \mathcal{F}' and classifier \mathcal{G} as our DeepFake detector $\mathcal{H}' = \mathcal{G} \circ \mathcal{F}'$.

E. Network Framework

Fig. 4 depicts the network architecture for our DeepFake detector. We design a ViT-based network as our feature extractor \mathcal{F} due to its strong power on vision tasks. Specifically, our feature extractor has two branches, a visual branch and a frequency branch. For the visual branch, we split the face image into 196 patches. These patches are flattened and linear transformed to patch embeddings, which are then equipped with position embeddings as the tokens for a ViT [29] architecture to extract visual features. The ViT in this branch contains l transformer layers, each of which is composed by a multi-headed self-attention (MSA) layer and a MLP layer [57]. For the frequency branch, we first convert the face image from RGB color space to YCbCr color space and then apply DCT transformation to each component with a 8×8 block [10]. The transformed frequency maps are concatenated together and sent into a convolution block. We then flatten the feature maps from the convolution block into 196 vectors, which are used as the input to another ViT architecture for frequency feature extraction. This ViT architecture contains m transformer layers. The visual features and frequency features are concatenated together as the forgery features for DeepFake detection. The classifier \mathcal{G} has a simple structure with only two linear layers, which takes the forgery features as input and outputs the logit of prediction. It is worth emphasizing that our method is independent of the network architecture, and can be integrated into other mainstream architectures. We use the architecture of Fig. 4 in our experiments as it can achieve

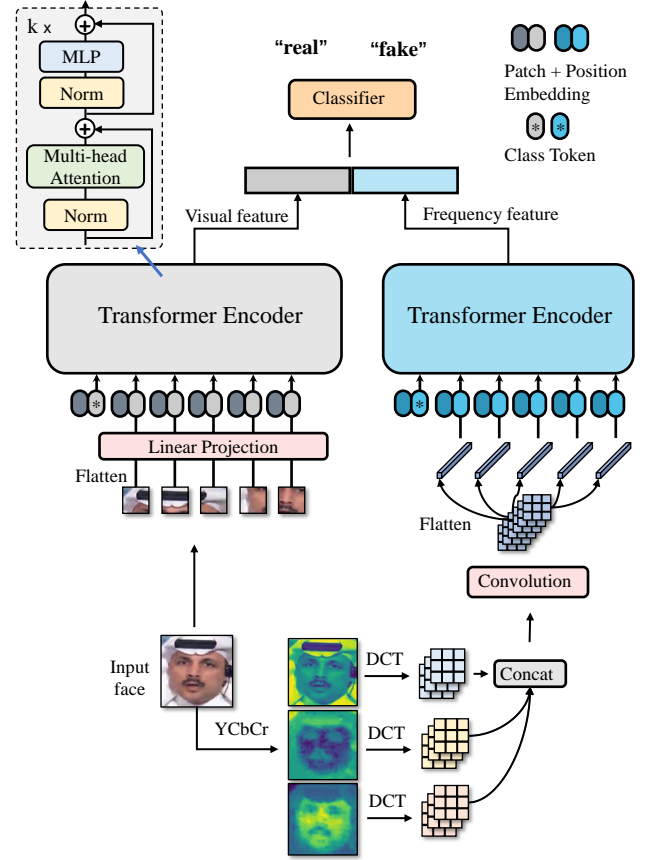


Fig. 4. Network architecture for DeepFake detector.

the best performance, which will be confirmed by Table ?? in Ablation Study.

IV. EXPERIMENTS

A. Experimental Settings

1) *Datasets:* We evaluate our approach on three public deepfake detection datasets, which are FF++ [13], Celeb-DF [14], and StyleGAN [58].

FF++ is a widely used dataset in deepfake detection. It includes 1,000 original videos from YouTube, covering a wide range of subjects and scenarios, and consists of four different manipulation techniques: Deepfakes (DF), Face2Face (F2F), FaceSwap (FS), and NeuralTextures (NT), each representing a distinct form of facial manipulation. All these videos have three compression versions, raw, high quality (HQ) and low quality (LQ). From these original videos, 720 videos, 140 videos and 140 videos are used for training, validating and testing, respectively. For each manipulation technique, we employ the same partition as the original videos for training, validating, and testing. We focus on the frame-level deepfake detection and perform evaluation on both HQ and LQ data. As our approach does not rely on extra augmentation operations, we only crop faces from each frame during the preprocessing stage. Concretely, we randomly extract 8 frames for each video clip and crop out the face with $1.3\times$ of the detection box obtained by RetinaFace [59].

Celeb-DF was proposed more recently, which provides a diverse set of challenges, such as pose, lighting conditions, fa-

cial expressions and camera quality, commonly encountered in real-world scenarios. It also offers different levels of manipulation difficulty, ranging from subtle and realistic manipulations to more obvious and noticeable ones. This dataset contains 590 original videos and 5639 DeepFake videos. We respectively use 5710 and 518 videos for training and testing. To construct the training data, we randomly extract 32 frames from real videos and 4 frames from fake videos for data balance. As for the testing set, we extract 16 frames from real and fake videos. The face is cropped out using the same way as for FF++.

StyleGAN [58] trains a generative adversarial network on Flickr-Faces-HQ dataset (FFHQ), which consists of 70000 real face images, to synthesize high-quality fake faces. The synthesizing process focuses on human faces and offers various high-quality synthetic faces by disentangling style and content information in latent space to control the process of face generation. We randomly select 2500 original images from FFHQ and 2500 synthetic images from the generated dataset, where 2000 original images and 2000 synthetic images are for training and the remaining images are for testing.

2) *Domain Adaptation Scenarios*: Since a new forgery can either be generated by a new manipulation method or come from an unseen data distribution, we design three adaptation scenarios, which are *Cross-manipulation-methods*, *Cross-manipulation-datasets* and *Cross-manipulation-types*, respectively. *Cross-manipulation-methods* is the case of crossing different manipulation methods in the same type (e.g., faceswap). *Cross-manipulation-datasets* represents the adaptation from one dataset to another different one. *Cross-manipulation-types* is to adapt one type of forgery to a different type. This scenario is more challenging, as different types have significant discrepancies in the manipulation methods, datasets and forged areas, e.g., faceswap faces to GAN-synthesized faces.

To make a fair comparison with the previous works [16], [35], each domain adaptation scenario is trained on the training set and tested on the testing set. Take the *Cross-manipulation-methods* scenario on FF++ dataset as an example. In training, we use the training set of source and target manipulation methods. In inference, we evaluate the trained model on the testing set of source and target manipulation methods. This configuration also applies to the other two scenarios.

3) *Implementation Details*: Following the design in Vit-Base [29], the feature extractor contains 12 (i.e., $l = 12$) transformer blocks, while we use 4 (i.e., $m = 12$) transformer blocks in frequency branch. The input images are resized to (224, 224). The weights of loss terms are set to $\alpha_1 = \alpha_2 = \alpha_3 = \alpha_4 = 1$. The training batch size is set to

TABLE I
THE PERFORMANCE OF OUR PROPOSED METHOD UNDER TWO CROSS-MANIPULATIONS SCENARIOS ON FF++. THE TOP PART IS THE RESULTS OF O2O AND THE BOTTOM PART IS THE RESULTS OF O2M.

Adaptation	DF	F2F	NT	FS
DF → F2F	99.00	99.08	66.21	64.67
DF → NT	87.88	60.02	95.03	43.49
DF → FS	98.82	75.68	57.41	99.37
F2F → DF	99.77	98.67	73.56	63.55
F2F → NT	89.89	95.59	95.85	57.11
F2F → FS	90.49	98.86	51.16	99.89
NT → DF	99.28	76.79	95.80	42.94
NT → F2F	92.79	97.44	93.27	63.74
NT → FS	78.96	63.28	70.05	97.81
FS → DF	98.90	79.62	61.16	98.95
FS → F2F	85.40	99.14	50.67	99.69
FS → NT	88.74	73.62	96.27	95.71
DF → F2F,NT,FS	97.64	98.64	88.73	99.12
F2F → DF,NT,FS	99.49	97.38	93.02	98.15
NT → DF,F2F,FS	98.90	97.20	94.52	95.35
FS → DF,F2F,NT	99.26	99.18	86.91	99.00

32 in forward adaptation and 24 in backward adaptation, as the teacher model occupy extra GPU memory. In the forward adaptation stage, we employ SGD as the optimizer, where the learning rate, momentum, and weight decay are set to 0.001, 0.9, and 0.0005, respectively. We stop the training of forward adaptation after 20 epochs. For backward adaptation, we set the learning rate to 0.0001 and the number of training epochs to 10. All experiments are conducted using Pytorch [60] on two Nvidia GTX 2080Ti GPUs.

B. Results of Cross-manipulation-methods

We investigate two settings in this scenario: one-to-one adaptation (O2O) and one-to-many adaptation (O2M). O2O uses one method as source and another one as target, while O2M uses one method as source and many other methods as target, which is more practical, as the collected target videos may have many new forgeries. All the experiments in this part are conducted on FF++ dataset and evaluated using the area under curve (AUC) metric.

1) *Performance of O2O and O2M*: In O2O, we select one of the four manipulation methods (DF, F2F, NT, FS) as the source domain and select a different method as the target domain. The top part of Table I shows the performance of our method under this O2O setting on the HQ set. Gray and yellow coloured values denote the performance on the source domain and target domain, respectively. The results

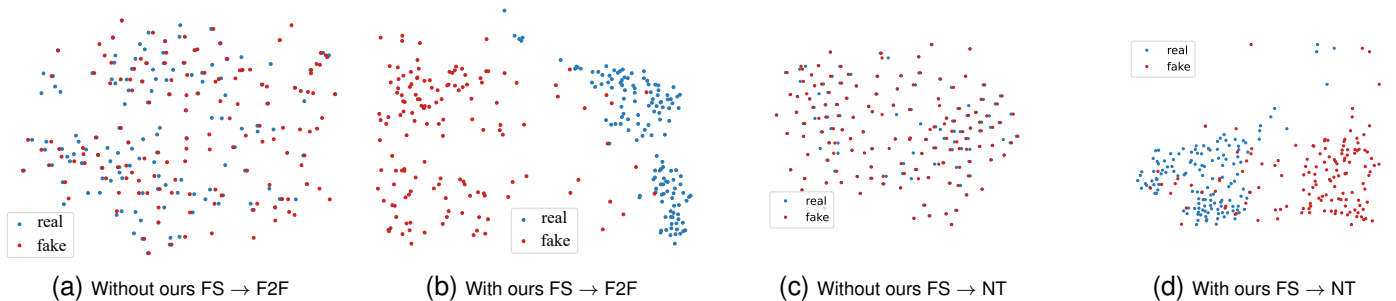


Fig. 5. T-SNE [65] visualization on FF++ (HQ).

TABLE II
COMPARISON OF OUR METHOD WITH STATE-OF-THE-ARTS UNDER O2O CROSS-MANIPULATION SCENARIO AT HQ LEVEL (TOP) AND LQ LEVEL (BOTTOM) IN FF++. THE BOLD NUMBER DENOTES THE BEST PERFORMANCE AND THE UNDERLINED ONE DENOTES THE SECOND BEST.

Method	DF			F2F			NT			FS		
	F2F	NT	FS	DF	NT	FS	F2F	DF	FS	F2F	NT	DF
(HQ) Face X-ray [16]	63.30	69.80	60.00	63.00	94.50	93.80	91.70	70.50	91.00	96.10	95.70	45.80
(HQ) SBI [18]	67.08	62.14	72.82	91.63	62.14	72.82	67.08	91.63	72.82	67.08	62.14	91.63
(HQ) LTW [34]	80.02	77.30	64.00	92.70	77.30	64.00	80.02	92.70	64.00	80.02	77.30	92.70
(HQ) Xception [13]	73.60	73.60	49.00	80.30	69.60	76.20	81.30	80.00	73.10	88.80	71.30	66.40
(HQ) SRM [21]	76.40	81.40	49.70	83.70	98.40	98.70	99.50	89.40	99.30	99.30	98.00	68.50
(HQ) SOLA-sup [63]	<u>97.29</u>	98.48	69.72	<u>99.73</u>	<u>96.02</u>	93.50	<u>97.69</u>	99.64	99.76	98.13	92.07	99.11
(HQ) FTCN [64]	-	-	-	98.00	96.00	95.90	-	-	-	-	-	-
(HQ) FOT [23]	-	-	-	-	-	72.57	-	-	-	-	-	-
(HQ) DDT [24]	-	64.10	-	-	-	-	-	78.82	-	-	-	-
(HQ) FEAT [54]	-	-	<u>88.62</u>	-	-	-	-	-	-	-	-	-
(HQ) Ours (O2O)	99.08	<u>95.03</u>	99.37	99.77	95.85	99.89	97.44	<u>99.28</u>	97.81	<u>99.14</u>	<u>96.27</u>	<u>98.90</u>
(LQ) SBI [18]	70.55	65.95	68.25	<u>85.60</u>	65.95	<u>68.25</u>	70.55	<u>85.60</u>	<u>68.25</u>	70.55	<u>65.95</u>	85.60
(LQ) FDFL [10]	58.90	63.61	66.87	67.55	55.35	66.66	74.21	79.09	74.21	54.64	49.72	75.90
(LQ) LTW [34]	72.40	60.80	68.10	75.60	60.80	68.10	72.40	75.60	68.10	72.40	60.80	75.60
(LQ) MATT [61]	66.41	66.01	67.33	73.04	71.88	65.10	80.61	74.56	60.90	61.65	54.79	82.33
(LQ) RECCE [62]	70.66	<u>67.34</u>	<u>74.29</u>	75.99	<u>72.32</u>	64.53	<u>80.89</u>	78.83	63.07	64.44	56.70	82.39
(LQ) Ours (O2O)	92.13	86.89	98.09	93.52	79.64	94.22	86.96	96.38	93.43	88.16	80.85	99.02

reveal that our method performs favourably on both source and target domains, achieving the AUC metric 95%+ on most of the source and target adaptation pairs. This demonstrates the effectiveness of our method. We also observe that the performance with NT \rightarrow FS is limited on the source. This is probably due to the large gap between NT and FS, and thus part of the knowledge in the source domain is lost.

In O2M, we select one manipulation method as source domain and use the other three methods as target domain. The performance achieved by our method are shown in the bottom part of Table I. We can observe that our method performs well on all the manipulation methods, which demonstrates that our method can learn the common forgery features even if the target domain is mixed with different manipulations.

Compared to the O2O scenario, O2M is more practical, as the daily emerged videos likely contain various manipulation methods. However, the foundation of O2M is O2O, as it still attempts to find the common knowledge among these various manipulation methods. Thus the O2O setting is also important, as it serves as the basis for the improvement of O2M.

2) *Comparison with State-of-the-Arts*: We compare our method with several state-of-the-art methods, including the augmentation-based methods (Face X-ray [16], SBI [18]), frequency-based methods (SRM [21], FDFL [10]), transfer-based methods (FOT [23], DDT [24], FEAT [54]), and other methods (Xception [13], MATT [61], LTW [34], RECCE [62], SOLA-sup [63], FTCN [64]).

We would like to clarify that the experiment configurations between our method and these other methods are different, as these methods tackle this task under different scenarios. Specifically, these data-level methods first obtain and empirically analyze the new forgery videos, and then summarize a common forgery knowledge as a prior, e.g., the blending boundary and frequency clues. By contrast, the prior knowledge for us is the collected videos without labels. Even though the experiment configurations are not the same, the results can also reflect the effectiveness of our method in exposing new forgeries.

Table II compares the performance of our method with those of the existing methods under the O2O scenario on both HQ and LQ levels, where the results of our method are marked by gray colour. For the existing methods, we use the score of each method reported in its original paper. As SBI [18] was only evaluated on raw quality images, we retrain it using the code provided in [18] on HQ and LQ for a fair comparison.

For the HQ level, it can be seen from the top part of Table II that our method outperforms the augmentation-based methods, Face X-ray and SBI, by a large margin. Since these two methods require prior knowledge of manipulation, they can hardly handle the forgery that has notable differences from the prior knowledge. The frequency-based method SRM performs well on several cases, notably, FS \rightarrow F2F and NT \rightarrow F2F. But its performances are highly degraded in many more cases compared to our method. For example, in DF \rightarrow FS, our method is nearly 100% better than SRM, and in FS \rightarrow DF, our method is 44% better than SRM, while in DF \rightarrow F2F, our method is 30% better than SRM, and in F2F \rightarrow DF, our method is 20% better than SRM. Similar observations can be drawn by comparing our method with SOLA-sup. Based on the available data from [64], the performance of our method are slightly better than those of FTCN. It can also be seen that our method significantly outperforms LTW, Xception, FOT, DDT and FEAT. Moreover, in the more challenging LQ level, our method significantly outperforms all the five benchmarks, as can be seen from the bottom part of Table II.

Fig. 5 shows the t-SNE [65] visualizations of feature distribution for two O2O cross-manipulations without and with adaptation using our method. It can be seen that the features of real and fake faces separate well using our method, in contrast to the mixed features without our method. Fig. 6 shows several examples of Grad-CAM [56] (the left six columns), which reveals that our method catches more discriminative features on face regions for both real and fake faces.

3) *Comparison with Existing UDA Methods*: As our approach draws inspiration from UDA to enhance the general-

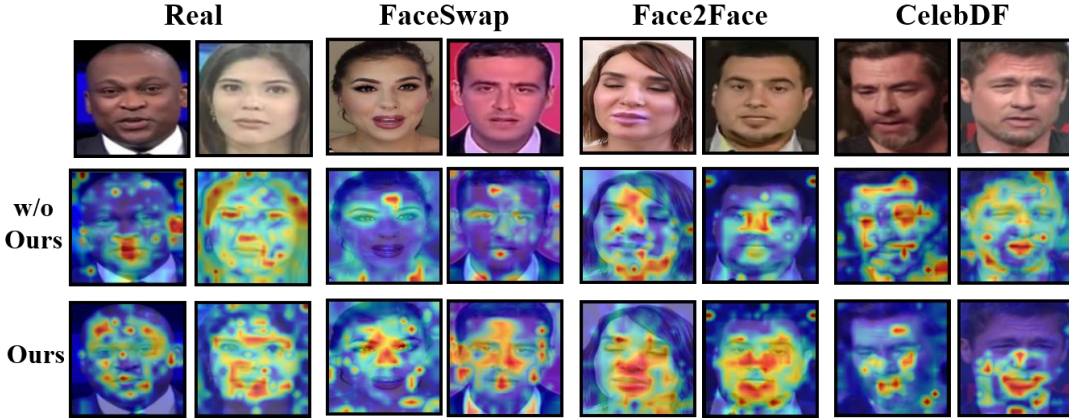


Fig. 6. Grad-CAM [56] visualization without and with adaptation using our method.

TABLE III
COMPARISON OF OUR METHOD WITH STATE-OF-THE-ARTS DOMAIN ADAPTATION METHODS. THE BOLD NUMBER DENOTES THE BEST PERFORMANCE.

Method	DF			F2F			NT			FS		
	F2F	NT	FS	DF	NT	FS	F2F	DF	FS	F2F	NT	DF
(HQ) SSRT [53]	51.43	50.36	61.79	86.79	49.64	50.36	54.64	90.71	49.29	58.21	50.00	86.43
(HQ) MDD [46]	71.79	73.57	61.79	80.36	70.00	80.71	77.50	88.93	75.00	75.71	50.37	73.93
(HQ) DANN [48]	95.71	90.71	94.29	94.99	88.57	96.43	90.36	92.86	89.64	91.43	87.14	95.00
(HQ) Ours (O2O)	99.08	95.03	99.37	99.77	95.85	99.89	97.44	99.28	97.81	99.14	96.27	98.90
(LQ) SSRT [53]	50.35	50.40	56.79	73.21	54.28	56.43	66.79	68.93	59.29	50.36	50.14	92.14
(LQ) MDD [46]	62.50	57.14	62.14	68.93	56.79	62.50	70.71	77.49	65.71	59.29	49.99	77.50
(LQ) DANN [48]	78.21	71.43	83.93	82.86	66.78	81.79	77.50	81.07	75.71	80.36	68.21	90.36
(LQ) Ours (O2O)	92.13	86.89	98.09	93.52	79.64	94.22	86.96	96.38	93.43	88.16	80.85	99.02

ization ability when facing unseen DeepFake techniques, we also perform a further comparison with the recently developed domain adaptation methods, SSRT [53], MDD [46] and DANN [48]. Specifically, we retrain their models on FF++ HQ and LQ scenarios by using their published codes. The experimental results are summarized in Table III, which demonstrate that our method outperforms these three domain adaptation methods in recognizing faces with unseen forgeries. SSRT [53] is a counterpart method that also employs a powerful vision transformer as the backbone network. It can be seen that SSRT occasionally fails to transfer knowledge in some scenarios, e.g., DF→NT and FS→F2F, while our bi-directional network achieves more stable and superior performance than SSRT almost in all adaptation tasks. DANN and MDD respectively represent an adversarial-based method and a discrepancy-based method. We observe that DANN achieves more generalized performance than MDD but our approach surpasses both DANN and MDD by a large margin. The reason mainly lies in that the proposed bi-directional adaptation strategy enables the model to fully grab the common forgery features across domains. Overall, the results suggest that our approach effectively encourages the detector to learn common forgery features, leading to improved generalization ability.

C. Results of Cross-manipulation-datasets

In this experiment, we use FF++ as source domain and Celeb-DF as target domain. Table IV compares our method with the state-of-the-art methods, F³-Net [19], MATT [61], RECCE [62], Two-branch [66], LTW [34], DSP-FWA [15],

MTD-Net [36], Xception [13], CFFs [37], DAM [67], SOLA-sup [63], SPSL [68], LiSiam [38], SLADD [35], LipForensics [69], HFI-Net [39], FTCN [64], F²Trans [40], and PCL+I2G [17]. It can be seen from Table IV that our method achieves

TABLE IV
PERFORMANCE COMPARISON OF OUR METHOD WITH STATE-OF-THE-ARTS UNDER CROSS-DATASETS SCENARIO FROM FF++ TO CELEB-DF. TRAINING SET FF++ INDICATES FF++ WITH FOUR MANIPULATION METHODS (DF,F2F,NT,FS) AS SOURCE, AND FF++(DF) MEANS FF++ WITH ONLY ONE MANIPULATION METHOD DF AS THE TRAINING SET.

Method	Training Set	Testing Set
		Celeb-DF
(HQ) LTW [34]	FF++	64.10
(HQ) DSP-FWA [15]	FF++	69.30
(HQ) MTD-Net [36]	FF++	70.12
(HQ) Xception [13]	FF++	73.04
(HQ) CFFs [37]	FF++	74.20
(HQ) DAM [67]	FF++	75.30
(HQ) SOLA-sup [63]	FF++(DF)	76.02
(HQ) SPSL [68]	FF++	76.88
(HQ) LiSiam [38]	FF++	78.21
(HQ) SLADD [35]	FF++	79.70
(HQ) LipForensics [69]	FF++	82.40
(HQ) HFI-Net [39]	FF++	83.28
(HQ) FTCN [64]	FF++	86.90
(HQ) F ² Trans [40]	FF++	89.87
(RAW) PCL+I2G [17]	FF++	90.03
(HQ) Ours	FF++	90.22
(LQ) F ³ -Net [19]	FF++	61.51
(LQ) MATT [61]	FF++	67.02
(LQ) RECCE [62]	FF++	68.71
(LQ) Two-branch [66]	FF++	73.41
(LQ) Ours	FF++	81.39

90.22% at HQ and 81.39% at LQ, respectively, outperforming all the other methods by a large margin. Note that PCL+I2G [17] synthesizes forged faces with raw quality data since the uncompressed data can provide more distinct features than the compression ones. This demonstrates that our method is capable of transferring the forgery knowledge from one dataset to another. The last two columns of Fig. 6 depict the examples of Grad-CAM from FF++ to Celeb-DF, which shows that our method concentrates more on forgery regions than the case without using our method.

TABLE V

PERFORMANCE COMPARISON OF OUR METHOD WITH STATE-OF-THE-ARTS UNDER CROSS-FACESWAP&GAN SCENARIO FROM FF++ TO STYLEGAN.

Method	DF	F2F	NT	FS	Avg.
(HQ) MATT [61]	43.99	43.99	43.99	43.99	43.99
(HQ) RECCE [62]	44.80	44.80	44.80	44.80	44.80
(HQ) SBI [18]	48.60	48.60	48.60	48.60	48.60
(HQ) Ours	68.55	58.06	55.10	59.08	60.20
(LQ) MATT [61]	32.51	32.51	32.51	32.51	32.51
(LQ) RECCE [62]	58.95	58.95	58.95	58.95	58.95
(LQ) SBI [18]	64.11	64.11	64.11	64.11	64.11
(LQ) Ours	71.07	52.51	88.62	70.28	70.62

D. Results of Cross-manipulation-types

In this part, we investigate the feasibility of our method to adapt faceswap faces to GAN-synthesized faces. Faceswap replaces the central region of face and retains other regions unchanged, while GAN synthesizes the whole face image. We use each of faceswap methods in FF++ [13] as source and adapt it to the StyleGAN dataset [58]. Table V shows the performance of our method in comparison to the three benchmark methods, MATT [61], RECCE [62] and SBI [18], under this setting. For fair comparison, we use the codes provided in [18], [61], [62] for SBI, MATT and RECCE under their defaulting settings. Observe that these three methods perform poorly, and in most cases their performance are below 50%. This is because these methods are designed to detect faceswap DeepFakes, e.g., finding the blending artifacts, and they cannot handle StyleGAN synthesized faces. In contrast, our method outperforms these methods by a large margin, on average 37%, 34% and 24% better at HQ level, and 117%, 20% and 10% better at LQ level, than MATT, RECCE and SBI, respectively. This is because our method focuses on learning the common forgery knowledge in the central regions of both faceswap and GAN DeepFakes, instead of simply exposing the faceswap-specific forgery features.

E. Ablation Study

We also conduct comprehensive ablation experiments to fully analyze the proposed method. More specifically, 1) validates the efficacy of proposed approach; 2) demonstrates the proposed method is data-efficient and can work with various backbone networks; and 3) shows that our method can also benefit other augmentation-based face forgery detection methods to improve their generalization ability.

TABLE VI
EFFECT OF VARIOUS ADAPTATION SETTINGS.

Method	DF \rightarrow F2F		DF \rightarrow FS		NT \rightarrow FS	
	DF	F2F	DF	FS	NT	FS
Baseline	99.32	57.98	99.53	76.18	87.61	53.45
+ GRL [70]	99.29	68.32	99.55	89.46	88.22	71.11
+ MMD [44]	99.22	84.12	99.52	94.76	87.63	83.88
+ FA	99.30	86.49	99.62	95.61	87.90	84.53
+ SD	97.85	90.59	96.02	98.57	77.53	95.89
+ Ent. [71]	74.89	54.98	68.73	54.92	55.67	50.67
Ours	96.43	92.13	98.08	98.09	85.03	93.94

1) *Various Adaptation Settings:* To provide more insights, we further investigate the proposed bi-directional adaptation strategy on the LQ set of FF++. We use the DeepFake detector trained on the source domain without adaptation as the baseline. GRL [70] and MMD [44] are two classical domain adaptation methods. GRL uses the gradient reversal layer and MMD attempts to reduce the distance of the probability distributions between source and target domains. GRL is exactly the domain adaptation method adopted in FEAT [54]. We denote the forward adaptation method in our method as FA. In the top part of Table VI, we evaluate these three domain adaptation methods. It can be seen that adding GRL, MMD or FA can improve the performance in the target domain, and using our FA attains the highest performance gain.

Then we take a further step to analyze the effect of backward adaptation in the bottom part of Table VI, where SD means that the self-distillation is used in backward adaptation, while Ent. represents that self-distillation is replaced with entropy minimization of samples, which is inspired by the method of [71]. We observe that only adding SD can notably improve the performance on the target domain, but its performance on the source domain is compromised, especially in NT \rightarrow FS, with 77.53% of +SD v.s. 87.61% of Baseline. This is because self-distillation is effective on the target domain, but overlooks the adaptation learned in forward adaptation. It can also be seen that replacing SD with Ent. is a bad idea, as this strategy degrades the detection performance in both domains. By adding both our forward adaptation and backward adaptation components to the baseline, our method can reach a good balance of the detection performance in both source and target domains. This clearly demonstrates that the proposed bi-directional adaptation is highly effective.

2) *Various Amounts of Training Samples:* This part investigates the data efficiency of the proposed method. We randomly select a proportion or percentage of the samples in target domain for training to simulate data-constrained

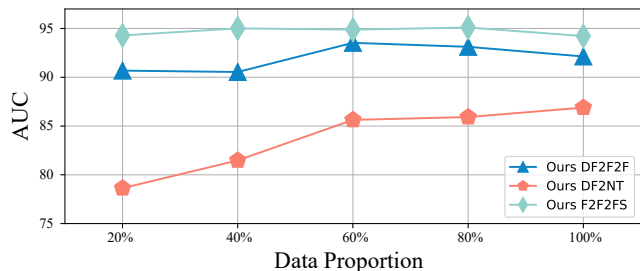


Fig. 7. Performance of using various amounts of training samples.

scenarios. Fig. 7 depicts the performance of our method for the adaptation pairs of DF \rightarrow F2F, DF \rightarrow NT, and F2F \rightarrow FS on the LQ set of FF++ using the percentage of the target samples ranging from 20% to 100%. As expected, increasing the percentage generally improves achievable performance. More importantly, noting the baseline+FA performance of 86.49 for DF \rightarrow F2F from Table VI, it can be seen that our method can still considerably enhance the performance to over 90 even if only 20% of target samples are used. This indicates that our method can be utilized in the more restricted cases where the available target samples are insufficient.

TABLE VII
EFFECT OF FREQUENCY MODULE.

Method	DF \rightarrow F2F		DF \rightarrow FS		NT \rightarrow FS	
	DF	F2F	DF	FS	NT	FS
C-192,D-4	93.34	90.36	96.56	97.51	80.97	92.69
C-384,D-4	95.26	90.65	97.82	97.66	84.13	93.46
C-768,D-2	95.17	90.97	96.97	97.35	84.21	92.39
C-768,D-3	95.70	91.21	97.86	96.87	84.23	92.78
C-768,D-4	96.43	92.13	98.08	98.09	85.03	93.94

3) *Effect of Frequency Module*: The number of channels (C) and depth (D) of DCT blocks are two important factors for extracting frequency features. The C and D values used in our method are 768 and 4. We now investigate the achievable performance of our method using various C and D values on the LQ set of FF++. As can be seen from Table VII, given depth D = 4, increasing channels from C = 192, 384 to 768 improves the achievable performance on both source and target domains. Likewise, with channels fixed to C = 768, increasing depth from D = 2, 3 to 4 improves the achievable performance on both domains. The results of Table VII also validate that our choice of C = 768 and D = 4 is appropriate.

TABLE VIII
PERFORMANCE OF USING VARIOUS FEATURE EXTRACTORS.

Method	DF \rightarrow F2F		DF \rightarrow FS		NT \rightarrow FS	
	DF	F2F	DF	FS	NT	FS
ResNet-50 [30]	99.40	57.51	99.40	65.72	87.72	57.27
ResNet-50 + Ours	96.89	76.17	96.49	90.61	77.99	71.21
Xception [31]	98.71	63.04	98.71	65.11	89.81	51.93
Xception + Ours	98.66	78.52	98.60	90.37	88.89	85.18
EfficientNet-B0 [32]	98.98	58.56	98.98	68.93	87.48	48.28
EfficientNet-B0 + Ours	90.26	91.24	98.32	94.66	84.45	91.57
EfficientNet-B4 [32]	98.82	57.91	98.82	68.63	88.77	48.56
EfficientNet-B4 + Ours	93.98	88.44	99.26	90.17	89.62	90.35
ViT-Small [29]	98.69	59.91	98.69	75.75	86.82	52.99
ViT-Small + Ours	95.63	87.46	97.27	95.58	83.83	83.17
ViT-Base [29]	99.32	57.98	99.53	76.18	87.61	53.45
ViT-Base + Ours	96.43	92.13	98.08	98.09	84.24	93.94

4) *Various Feature Extractors*: As mentioned in the introduction section, the proposed framework is independent of the architecture. Table VIII shows the performance of applying our framework on ResNet-50 [30], Xception [31], EfficientNet-B0 [32], EfficientNet-B4 [32], ViT-small [29] and ViT-base [29] on the LQ set of FF++. It can be seen that for each base network, our method significantly improves the performance on the target domain while maintaining a favorable performance on the source domain. This demonstrates that our proposed method is generically applicable.

5) *Added on State-of-the-art DeepFake Detection*: This part investigates the effectiveness of our method to improve recently developed advanced detection methods. We use SBI [18] as an example. Specifically, we retrain SBI with HQ and LQ faces in FF++, and compare it with our method added on SBI. In this experiment, the source domain consists of fake faces blended by SBI and pristine faces and the target domain is each manipulation method. The results shown in Table IX reveal that with our method added on, SBI notably improves the performance both at HQ and LQ levels. This indicates that our method can be easily integrated into other detection methods to enhance their generalization ability.

TABLE IX
PERFORMANCE OF ADDING OUR METHOD ON SBI.

Method	DF	F2F	NT	FS	Avg.
(HQ) SBI [18]	85.88	80.07	72.47	75.62	78.51
(HQ) SBI + Ours	99.00	97.23	90.28	92.92	94.86
(LQ) SBI [18]	80.70	67.63	65.13	62.50	68.99
(LQ) SBI + Ours	88.93	68.20	64.98	65.52	71.91

V. CONCLUSIONS

This paper has proposed a new framework to detect new forgeries across different domains, called *DomainForensics*. Different from the recent methods, which empirically seeks the common traces on data view, our method aims to transfer the forgery knowledge from known forgeries (fully labeled source domain) to new forgeries (label-free target domain). Since the general domain adaptation methods are not competent to capture the forgery features, we have designed a new bi-directional adaptation strategy that considers both the forward adaptation and backward adaptation. Specifically, the forward adaptation transfers the knowledge from the source to the target domain, and the backward adaptation reverses the adaptation from the target to the source domain. With this backward adaptation, the detector can be further enhanced to learn new forgery features from unlabeled data and avoid forgetting the known knowledge of known forgery. Extensive experiments have been conducted on three datasets with the comparison to several existing state-of-the-art counterparts. The results obtained have demonstrated that our method is effective in exposing new forgeries, and it can be integrated into various architectures to improve their generalization ability.

REFERENCES

- [1] I. Goodfellow, *et al.*, "Generative adversarial nets," in *Proc. NIPS 2014* (Montreal, Quebec, Canada), Dec. 8-13, 2014, pp. 1-9.
- [2] J. Thies, *et al.*, "Face2Face: Real-time face capture and reenactment of RGB videos," in *Proc. CVPR 2016* (Las Vegas, NV, USA), Jun. 26-Jul. 1, 2016, pp. 2387-2395.
- [3] S. Suwajanakorn, S. M. Seitz, and I. Kemelmacher-Shlizerman, "Synthesizing Obama: Learning lip sync from audio," *ACM Trans. Graphics*, vol. 36, no. 4, article no. 95, pp. 1-13, 2017.
- [4] H. Kim, *et al.*, "Deep video portraits," *ACM Trans. Graphics*, vol. 37, no. 4, article no. 163, pp. 1-14, 2018.
- [5] T. Karras, T. Aila, S. Laine, and J. Lehtinen, "Progressive growing of GANs for improved quality, stability, and variation," in *Proc. ICLR 2018* (Vancouver, BC, Canada), Apr. 30-May 3, 2018, pp. 1-26.
- [6] T. Karras, S. Laine, and T. Aila, "A style-based generator architecture for generative adversarial networks," in *Proc. CVPR 2019* (Long Beach, CA, USA), Jun. 16-20, 2019, pp. 4401-4410.

- [7] R. Chesney and D. K. Citron, "Deep Fakes: A looming challenge for privacy, democracy, and national security," *California Law Review*, vol. 107, no. 6, pp. 1753–1820, 2019.
- [8] Y. Li, M.-C. Chang, and S. Lyu, "In Ictu Oculi: Exposing AI generated fake face videos by detecting eye blinking," in *Proc. WIFS 2018* (Hong Kong, China), Dec. 11-13, 2018, pp. 1–7.
- [9] D. Afchar, V. Nozick, J. Yamagishi, and I. Echizen, "MesoNet: A compact facial video forgery detection network," in *Proc. WIFS 2018* (Hong Kong, China), Dec. 11-13, 2018, pp. 1–7.
- [10] J. Li, *et al.*, "Frequency-aware discriminative feature learning supervised by single-center loss for face forgery detection," in *Proc. CVPR 2021*, Jun. 19-25, 2021, pp. 6458–6467.
- [11] Z. Sun, *et al.*, "Improving the efficiency and robustness of deepfakes detection through precise geometric features," in *Proc. CVPR 2021*, Jun. 19-25, 2021, pp. 3609–3618.
- [12] Y. He, *et al.*, "ForgeryNet: A versatile benchmark for comprehensive forgery analysis," in *Proc. CVPR 2021*, Jun. 19-25, 2021, pp. 4358–4367.
- [13] A. Rössler, *et al.*, "FaceForensics++: Learning to detect manipulated facial images," in *Proc. ICCV 2019* (Seoul, South Korea), Oct. 27-Nov. 2, 2019, pp. 1–11.
- [14] Y. Li, *et al.*, "Celeb-DF: A large-scale challenging dataset for deepfake forensics," in *Proc. CVPR 2020*, Jun. 14-19, 2020, pp. 3207–3216.
- [15] Y. Li and S. Lyu, "Exposing deepfake videos by detecting face warping artifacts," in *Proc. CVPRW, 2019* (Long Beach, CA, USA), Jun. 16-17, 2019, pp. 46–52.
- [16] L. Li, *et al.*, "Face X-ray for more general face forgery detection," in *Proc. CVPR 2020*, Jun. 14-19, 2020, pp. 5001–5010.
- [17] T. Zhao, *et al.*, "Learning self-consistency for deepfake detection," in *Proc. ICCV 2021*, Oct. 11-17, 2021, pp. 15023–15033.
- [18] K. Shiohara and T. Yamasaki, "Detecting deepfakes with self-blended images," in *Proc. CVPR 2022* (New Orleans, LA, USA), Jun. 19-24, 2022, pp. 18720–18729.
- [19] Y. Qian, *et al.*, "Thinking in frequency: Face forgery detection by mining frequency-aware clues," in *Proc. ECCV 2020* (Glasgow, UK), Aug. 23-28, 2020, pp. 1–18.
- [20] H. Liu, *et al.*, "Spatial-phase shallow learning: Rethinking face forgery detection in frequency domain," in *Proc. CVPR 2021*, Jun. 19-25, 2021, pp. 772–781.
- [21] Y. Luo, Y. Zhang, J. Yan, and W. Liu, "Generalizing face forgery detection with high-frequency features," in *Proc. CVPR 2021*, Jun. 19-25, 2021, pp. 16317–16326.
- [22] C. Dong, A. Kumar, and E. Liu, "Think twice before detecting GAN-generated fake images from their spectral domain imprints," in *Proc. CVPR 2022* (New Orleans, LA, USA), Jun. 18-24, 2022, pp. 7855–7864.
- [23] D. Cozzolino, *et al.*, "ForensicTransfer: Weakly-supervised domain adaptation for forgery detection," *arXiv:1812.02510*, 2018.
- [24] S. Aneja and M. Nießner, "Generalized zero and few-shot transfer for facial forgery detection," *arXiv:2006.11863*, 2020.
- [25] H. Qiu, *et al.*, "Few-shot forgery detection via guided adversarial interpolation," *Pattern Recognition*, vol. 144, article no. 109863, pp. 1–11, Dec. 2023.
- [26] H. Wang, X. Guo, Z.-H. Deng, and Y. Lu, "Rethinking minimal sufficient representation in contrastive learning," in *Proc. CVPR 2022* (New Orleans, LA, USA), Jun. 18-24, 2022, pp. 16041–16050.
- [27] T. Chen, *et al.*, "Big self-supervised models are strong semi-supervised learners," in *Proc. NeurIPS 2020*, Dec. 6-12, 2020, pp. 1–13.
- [28] Z. Li, *et al.*, "One-class knowledge distillation for face presentation attack detection," *IEEE Trans. Information Forensics and Security*, vol. 17, pp. 2137–2150, Jun. 2022.
- [29] A. Dosovitskiy, *et al.*, "An image is worth 16x16 words: Transformers for image recognition at scale," in *Proc. ICLR 2021*, May 3-7, 2021, pp. 1–21.
- [30] K. He, X. Zhang, S. Ren, and J. Sun, "Deep residual learning for image recognition," in *Proc. CVPR 2016* (Las Vegas, NV, USA), Jun. 26-Jul. 1, 2016, pp. 770–778.
- [31] F. Chollet, "Xception: Deep learning with depthwise separable convolutions," in *Proc. CVPR 2017* (Honolulu, HI, USA), Jul. 21-26, 2017, pp. 1251–1258.
- [32] M. Tan and Q. Le, "EfficientNet: Rethinking model scaling for convolutional neural networks," in *Proc. ICML 2019* (Long Beach, CA, USA), Jun. 10-15, 2019, pp. 1–11.
- [33] S. Agarwal, *et al.*, "Protecting world leaders against deep fakes," in *Proc. CVPR 2019 Workshops* (Long Beach, CA, USA), Jun. 16-20, 2019, pp. 38–45.
- [34] K. Sun, *et al.*, "Domain general face forgery detection by learning to weight," in *Proc. AAAI 2021*, Feb. 2-9, 2021, pp. 2638–2646.
- [35] L. Chen, *et al.*, "Self-supervised learning of adversarial example: Towards good generalizations for deepfake detection," in *Proc. CVPR 2022* (New Orleans, LA, USA), Jun. 19-24, 2022, pp. 18710–18719.
- [36] J. Yang, *et al.*, "MTD-Net: Learning to detect deepfakes images by multi-scale texture difference," *IEEE Trans. Information Forensics and Security*, vol. 16, pp. 4234–4245, Aug. 2021.
- [37] P. Yu, *et al.*, "Improving generalization by commonality learning in face forgery detection," *IEEE Trans. Information Forensics and Security*, vol. 17, pp. 547–558, Feb. 2022.
- [38] J. Wang, Y. Sun, and J. Tang, "LiSiam: Localization invariance Siamese network for deepfake detection," *IEEE Trans. Information Forensics and Security*, vol. 17, pp. 2425–2436, Jul. 2022.
- [39] C. Miao, *et al.*, "Hierarchical frequency-assisted interactive networks for face manipulation detection," *IEEE Trans. Information Forensics and Security*, vol. 17, pp. 3008–3021, Aug. 2022.
- [40] C. Miao, *et al.*, "F²Trans: High-frequency fine-grained transformer for face forgery detection," *IEEE Trans. Information Forensics and Security*, vol. 18, pp. 1039–1051, Jan. 2023.
- [41] X. Zhu, *et al.*, "Face forgery detection by 3D decomposition," in *Proc. CVPR 2021*, Jun. 19-25, 2021, pp. 2929–2939.
- [42] S. Ben-David, J. Blitzer, K. Crammer, and F. Pereira, "Analysis of representations for domain adaptation," in *Proc. NIPS 2006* (Vancouver, BC, Canada), Dec. 4-9, 2006, pp. 1–8.
- [43] E. Tzeng, *et al.*, "Deep domain confusion: Maximizing for domain invariance," *arXiv:1412.3474*, 2014.
- [44] M. Long, Y. Cao, J. Wang, and M. Jordan, "Learning transferable features with deep adaptation networks," in *Proc. ICML 2015* (Lille, France), Jul. 6-11, 2015, pp. 97–105.
- [45] B. Sun and K. Saenko, "Deep CORAL: Correlation alignment for deep domain adaptation," in *Proc. ECCV 2016 Workshops* (Amsterdam, The Netherlands), Oct. 8-10 and Oct. 15-16, 2016, pp. 443–450.
- [46] Y. Zhang, T. Liu, M. Long, and M. I. Jordan, "Bridging theory and algorithm for domain adaptation," in *Proc. ICML 2019* (Long Beach, CA, USA), Jun. 9-15, 2019, pp. 7404–7413.
- [47] I. Goodfellow, *et al.*, "Generative adversarial networks," *Communications of the ACM*, vol. 63, no. 11, pp. 139–144, 2020.
- [48] Y. Ganin, *et al.*, "Domain-adversarial training of neural networks," *J. Machine Learning Research*, vol. 17, no. 1, pp. 2096–2030, 2016.
- [49] E. Tzeng, J. Hoffman, K. Saenko, and T. Darrell, "Adversarial discriminative domain adaptation," in *Proc. CVPR 2017* (Honolulu, HI, USA), Jul. 21-26, 2017, pp. 7167–7176.
- [50] M. Xu, *et al.*, "Adversarial domain adaptation with domain mixup," in *Proc. AAAI 2020* (New York, NY, USA), Feb. 7-12, 2020, pp. 6502–6509.
- [51] J. Yang, J. Liu, N. Xu, and J. Huang, "TVT: Transferable vision transformer for unsupervised domain adaptation," in *Proc. WACV 2023* (Waikoloa, HI, USA), Jan. 3-7, 2023, pp. 520–530.
- [52] T. Xu, *et al.*, "CDTrans: Cross-domain transformer for unsupervised domain adaptation," *arXiv:2109.06165*, 2021.
- [53] T. Sun, C. Lu, T. Zhang, and H. Ling, "Safe self-refinement for transformer-based domain adaptation," in *Proc. CVPR 2022* (New Orleans, LA, USA), Jun. 19-24, 2022, pp. 7191–7200.
- [54] B. Chen and S. Tan, "FeatureTransfer: Unsupervised domain adaptation for cross-domain deepfake detection," *Security and Communication Networks*, vol. 2021, article 9942754, pp. 1–8, 2021.
- [55] Y. Li, X. Bian, M.-C. Chang, and S. Lyu, "Exploring the vulnerability of single shot module in object detectors via imperceptible background patches," in *Proc. BMVC 2019* (Cardiff, UK), Sep. 9-12, 2019, pp. 1–12.
- [56] R. R. Selvaraju, *et al.*, "Grad-CAM: Visual explanations for deep networks via gradient-based localization," in *Proc. ICCV 2017* (Venice, Italy), Oct. 22-29, 2017, pp. 618–626.
- [57] A. Vaswani, *et al.*, "Attention is all you need," *Proc. NIPS 2017* (Long Beach, CA, USA), Dec. 4-9, 2017, pp. 1–11.
- [58] T. Karras, S. Laine, and T. Aila, "A style-based generator architecture for generative adversarial networks," *IEEE Trans. Pattern Analysis and Machine Intelligence*, vol. 43, no. 12, pp. 4217–4228, Dec. 2021.
- [59] J. Deng, *et al.*, "RetinaFace: Single-shot multi-level face localisation in the wild," in *Proc. CVPR 2020* (Seattle, WA, USA), Jun. 13-19, 2020, pp. 5202–5211.
- [60] A. Paszke, *et al.*, "Automatic differentiation in pytorch," in *Proc. NIPS 2017* (Long Beach, CA, USA), Dec. 4-9, 2017, pp. 1–4.
- [61] H. Zhao, *et al.*, "Multi-attentional deepfake detection," in *Proc. CVPR 2021*, Jun. 19-25, 2021, pp. 2185–2194.

- [62] J. Cao, *et al.*, “End-to-end reconstruction-classification learning for face forgery detection,” in *Proc. CVPR 2022* (New Orleans, LA, USA), Jun. 18-24, 2022, pp. 4113–4122.
- [63] J. Fei, *et al.*, “Learning second order local anomaly for general face forgery detection,” in *Proc. CVPR 2022* (New Orleans, LA, USA), Jun. 18-24, 2022, pp. 20270–2080.
- [64] Y. Zheng, *et al.*, “Exploring temporal coherence for more general video face forgery detection,” in *Proc. ICCV 2021*, Oct. 11-17, 2021, pp. 15044–15054.
- [65] L. Van der Maaten and G. Hinton, “Visualizing data using t-SNE.” *J. Machine Learning Research*, vol. 9, article 86, pp. 2579–2605, 2008.
- [66] I. Masi, *et al.*, “Two-branch recurrent network for isolating deepfakes in videos,” in *Proc. ECCV 2020* (Glasgow, UK), Aug. 23-28, 2020, pp. 667–684.
- [67] T. Zhou, W. Wang, Z. Liang, and J. Shen, “Face forensics in the wild,” in *Proc. CVPR 2021*, Jun. 19-25, 2021, pp. 5778–5788.
- [68] H. Liu, *et al.*, “Spatial-phase shallow learning: Rethinking face forgery detection in frequency domain,” in *Proc. CVPR 2021*, Jun. 19-25, 2021, pp. 772–781.
- [69] A. Haliassos, K. Vougioukas, S. Petridis, and M. Pantic, “Lips don’t lie: A generalisable and robust approach to face forgery detection,” in *Proc. CVPR 2021*, Jun. 19-25, 2021, pp. 5039–5049.
- [70] Y. Ganin and V. Lempitsky, “Unsupervised domain adaptation by back-propagation,” in *Proc. ICML* (Lille, France), Jul. 6-11, 2015, pp. 1180–1189.
- [71] Y. Grandvalet and Y. Bengio, “Semi-supervised learning by entropy minimization,” in *Proc. NIPS 2004* (Vancouver, BC, Canada), Dec. 1, 2004, pp. 529–536.